



ENVIRONMENTAL RESEARCH BRIEF

Multiphase Chemical Transport in Porous Media

J.F. Guarnaccia¹, P.T. Imhoff¹, B.C. Missildine², M. Oostrom²,
M.A. Celia^{1*}, J.H. Dane^{2*}, P.R. Jaffé^{1*}, and G.F. Pinder^{3*}

Introduction

The contamination of groundwater by both lighter and heavier than water nonaqueous phase liquids (NAPLs) is a well-documented problem. Trichloroethylene is an example of a commonly encountered heavier than water or dense NAPL (DNAPL). Because DNAPLs are more dense than water, they sink through the aqueous phase until reaching an impermeable barrier, leaving a residual phase behind the advancing front. The trapped residual in the saturated zone remains essentially immobile, slowly dissolving into the flowing groundwater. This residual DNAPL acts as a long-term source of groundwater contamination.

This investigation focuses on the simulation of the emplacement and subsequent dissolution of a DNAPL in a saturated groundwater system. The final output of this project consists of a model that includes two distinct flow and transport processes. First is the emplacement of DNAPL in the subsurface. Here two-phase flow dominates as the DNAPL displaces the water. In addition, as the trailing edge of the slug of DNAPL migrates into the system, it leaves behind an immobile residual held in place by capillary forces. Contamination via this scenario occurs over a relatively small portion of the area of interest and encompasses relatively short time scales (on the order of

days). The second flow and transport process involves the dissolution of the immobile residual DNAPL through interfacial mass exchange and transport of the dissolved contaminant in the water phase. Contamination via this scenario can occur over a relatively large areal extent; and because dissolution is a slow process, the source for the contaminant can persist for long periods of time (on the order of years).

Numerical simulations of this problem are computationally intensive involving the iterative simultaneous solution of coupled nonlinear partial differential equations over fine time and space discretizations. In addition, validity of the model is dependent on knowledge of a series of physically based relationships that have to be determined experimentally. This communication presents an overview of the tasks undertaken to develop an efficient numerical simulator to study the DNAPL emplacement/dissolution problem. These tasks include: 1) the development of the governing equations which describe the flow-dissolution-transport process; 2) the experimental determination of the empirical constitutive relationships between capillary pressure and relative saturation for one representative DNAPL, trichloroethylene (TCE); 3) the experimental determination of an empirical model for TCE dissolution; 4) an examination of the numerical schemes necessary to model two-phase flow and associated dissolved transport, and the subsequent development of a numerical simulator from this study; and finally 5) the verification of the numerical simulator using analytical and experimental results.

Governing Equations/Constitutive Relations

The mass balance equations describing the simultaneous flow of two semi-miscible phases, one wetting (w, e.g., water) and

¹ Department of Civil Engineering and Operations Research,
Princeton University, Princeton, NJ 08544
² Department of Agronomy and Soils, Auburn University,
Auburn, AL 36849
³ Office of the Dean of Engineering and Mathematics,
University of Vermont, Burlington, VT 05405
* Principal Investigators



one nonwetting (n, e.g., DNAPL), under isothermal, incompressible conditions are written as a set of four coupled equations (following Pinder and Abriola, 1986):

- two-phase (α) mass balance equations:

$$\frac{\partial(\epsilon \rho^\alpha S_\alpha)}{\partial t} + \nabla \cdot [\epsilon \rho^\alpha S_\alpha \mathbf{v}^\alpha] = \rho^\alpha q^\alpha + \hat{\rho}^\alpha, \quad \alpha = w, n \quad (1a)$$

- two dissolved constituent (i, α) mass balance equations:

$$\frac{\partial(\epsilon S_\alpha \rho_i^\alpha)}{\partial t} + \nabla \cdot (\epsilon S_\alpha \rho_i^\alpha \mathbf{v}^\alpha) - \nabla \cdot [\epsilon S_\alpha D^\alpha \nabla \rho_i^\alpha] = \rho_i^\alpha q^\alpha + \hat{\rho}_i^\alpha \quad (1b)$$

where the constituents (i, α) are a DNAPL species (o) dissolved in the wetting phase (o, w) and a water species (w) dissolved in the nonwetting phase (w, n). The terms in equations (1) are:

- ρ_i^α = mass concentration of species i in the α phase, $[M/L^3]$
- ρ^α = α phase density, $[M/L^3]$, in general a function of composition
- S_α = α phase saturation, defined such that $S_w + S_n = 1$
- ϵ = the porosity of the porous medium
- \mathbf{v}^α = the mass average α phase velocity $[L/T]$ vector defined as:

$$\mathbf{v}^\alpha = -\frac{k k_{r\alpha}}{\epsilon S_\alpha \mu^\alpha} (\nabla P^\alpha - \rho^\alpha \mathbf{g}), \quad \alpha = w, n \quad (2)$$

with k = the intrinsic permeability tensor $[L^2]$,

- $k_{r\alpha}$ = the relative permeability which is a function of S_w
- μ^α = kinematic viscosity of the α phase $[FT/L^2]$, in general a function of fluid composition
- P^α = pressure in the α phase $[F/L^2]$
- \mathbf{g} = gravitational acceleration vector $[L/T^2]$
- D^α = the α phase hydrodynamic dispersion tensor $[L^2/T]$
- q^α = external source $[1/T]$, positive for influx and negative for efflux
- $\hat{\rho}_i^\alpha$ = interface mass exchange term $[M/L^3T]$ defined as:

$$\hat{\rho}_i^\alpha = C^{wn} (K_i^\alpha - \rho_i^\alpha), \quad \alpha = w, n \quad (3)$$

C^{wn} = the mass transfer rate coefficient $[1/T]$ between the wetting and nonwetting phases, in general a function of fluid saturation, composition and velocity; physical and chemical properties of the species (i) and phases (w and n); and the porous media properties

K_i^α = the solubility limit $[M/L^3]$ of species i in the α phase, in general a function of fluid composition

$\hat{\rho}^\alpha = \hat{\rho}_o^\alpha + \hat{\rho}_w^\alpha, [M/L^3T]$, the total mass flux into or out of the α phase where in this case $\hat{\rho}^n = -\hat{\rho}^w$

To close the system, two nonlinear material relationships must be provided. These are the relationships between capillary pressure, P_c ($P_c = P^n - P^w$), and saturations, S_α , and between relative permeabilities, $k_{r\alpha}$, and saturations, S_α . This development employs the van Genuchten $k_{r\alpha} - S_\alpha - P_c^\alpha$ (K-S-P) model described in Luckner et al. (1989) and written here as:

$$\bar{S}_w = \frac{S_w - S_{wr}}{1.0 - S_{wr}}, \quad (0 \leq \bar{S}_w \leq 1) \quad (4a)$$

$$\bar{S}_n = \frac{(1 - S_{nr}) - S_w}{1.0 - S_{nr}}, \quad (0 \leq \bar{S}_w \leq 1) \quad (4b)$$

$$\bar{S}_w = \frac{1}{[1 + (ah)^\eta]^m} \quad (4c)$$

$$k_{rw}(S_w) = (\bar{S}_w)^{1/2} [1 - (1 - \bar{S}_w)^{1/m}]^2 \quad (4d)$$

$$k_{rn}(S_w) = (\bar{S}_n)^{1/2} [1 - (1 - \bar{S}_n)^{1/m}]^{2m} \quad (4e)$$

where \bar{S}_w is the effective wetting phase saturation, S_{wr} is the residual wetting phase saturation, \bar{S}_n is the effective nonwetting phase saturation, S_{nr} is the residual nonwetting phase saturation, $h = (P_c/\rho_w g)$ is the capillary pressure head $[L]$, η [dimensionless] and a $[1/L]$ are porous medium dependent parameters to be fit to data, and $m = (1 - 1/\eta)$. Measurement of the fitting parameters, η and a , is described below; appropriate data are also given below. For the special case where one of the fluid phases is present at a saturation at or below its residual saturation, there is only one mobile fluid, and the capillary pressure - saturation becomes meaningless. Treatment of this

case, which has direct relevance to the problem of dissolving residual NAPLs, is discussed in the Numerical Methods section below. Treatment of hysteresis in the capillary pressure - saturation relation is also discussed in that section.

An Improved Method for the Determination of Capillary Pressure - Saturation Curves Involving Trichloroethylene, Water, and Air

An essential component in understanding and simulating multiphase fluid flow is the accurate determination of the hydraulic properties of the different fluids involved. It has been standard procedure to use pressure cells (Lenhard and Parker, 1987; Turrin, 1988; Demond and Roberts, 1991) to determine capillary pressure (P_c) - saturation (S_w) curves, where $P_c = P^n - P^w = 2\sigma/r$ (σ is the interfacial tension and r is the radius of curvature at the interface of two fluids). Because the interfacial tension between trichloroethylene (TCE) and air at 20°C is only 30 mN/m, and between TCE and water 38 mN/m, as compared to 72 mN/m between water and air, the height of the pressure cell may be critical during the displacement of one fluid by another if S_w changes rapidly with small changes in P_c , as is the case for coarser materials. The main objective of this part of the study was therefore to explore an improved way to determine P_c - S_w curves for TCE/air and TCE/water for a sand during imbibition and drainage cycles (hysteresis loops). Two additional factors of importance, for simulation and cleanup purposes, are the P_c values at which the nonwetting fluid starts to displace the wetting fluid and the values for the residual saturation of TCE in

TCE/air and TCE/water systems. These values were determined as well.

Materials and Methods

A 1 m long column experiment was designed to allow accurate P_c - S_w information to be collected at any given point of interest. The glass column (i.d. = 7.5 cm), with Teflon end caps, was filled uniformly with Flintshot 2.8 Ottawa sand. The outlet at the bottom of the column was connected to a supply (or drainage) bottle by Teflon tubing. This bottle, partially filled with TCE, was also used to adjust the fluid pressures in the column by lowering or raising it.

For the TCE/air combination, the sand column was subjected to the following cycles:

- Saturation from the bottom, by slowly raising the bottle, until TCE was ponded on the surface.
- TCE displaced by air by stepwise lowering the bottle.
- Air displaced by TCE by stepwise raising the bottle.
- Upon reaching equilibrium after each step change (no more flow), dual-energy gamma radiation measurements were taken at the desired locations to determine the volumetric content of TCE; θ_w (Oostrom and Dane, 1990).

P_c values were obtained from knowledge of the height of the TCE level in the supply/drainage bottle. Corresponding S_w values were calculated from $S_w = \theta_w/\epsilon$. A simplified schematic of the experimental setup is presented in Figure 1, with the TCE level

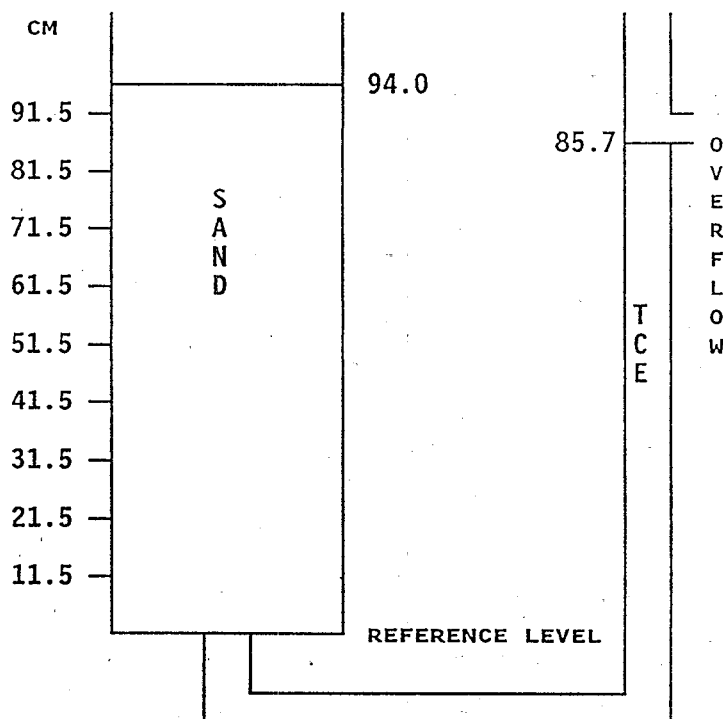


Figure 1. Simplified schematic of experimental setup. The surface of the sand column was 94.0 cm above the reference level (bottom of column). The TCE level in the supply/drainage bottle (indicated as overflow) was for this particular case at 85.7 cm.

In the overflow tube for this particular case at 85.7 cm above the reference level (bottom of sand column). By matching the corresponding P_c and S_w values, $P_c - S_w$ data points were obtained.

Upon completion of the TCE/air experiments, a 2 cm layer of water was maintained on the soil surface to displace the TCE by water, or vice versa, and $P_c - S_w$ curves were determined for TCE/water in a similar manner as described for TCE/air. The dual-energy gamma radiation system now determined both the volumetric TCE content, θ_n , and the volumetric water content, θ_w .

The $P_c - S_w$ data were fitted with the van Genuchten curve fitting procedure (equations 4). The P_c entry value for the nonwetting fluid was taken as $1/a$, where a is a curve fitting parameter.

Results and Discussion

TCE saturation data (S_w) during the displacement of TCE by air (TCE draining), are shown in Figure 2. The solid line is the curve as fitted by the van Genuchten procedure ($a = 0.148$, $\eta = 7.244$, $S_{wr} = 0.059$, and saturated $S_w = 0.817$). The data points obtained during the displacement of air by TCE (TCE imbibing) and the fitted van Genuchten curve are shown in Figure 3 ($a = 0.220$, $\eta = 6.657$, $S_{wr} = 0.059$, and saturated $S_w = 0.742$). To appreciate the amount of hysteresis, the fitted van Genuchten

functions are shown, without the data points, in Figure 4. It can easily be seen in Figures 2, 3, and 4 that S_w changes from its maximum to its minimum value, and vice versa, over a capillary pressure difference of about 5.5 cm of equivalent water pressure. The data also show that ignoring hysteresis can have a profound effect on S_w . Similar graphs were obtained during the displacement of TCE by water (Figure 5: water imbibing, $a = 0.216$, $\eta = 13.752$, $S_{wr} = 0.0$, and saturated $S_w = 0.763$) and for the displacement of water by TCE (Figure 6: water draining, $a = 0.078$, $\eta = 10.457$, $S_{wr} = 0.093$, and saturated $S_w = 0.770$). The fitted van Genuchten functions for the water/TCE system are separately displayed in Figure 7. The change in S_w with capillary pressure is again very rapid, especially for the (water) imbibition curve. The amount of hysteresis in this case is even more pronounced than for the TCE/air system.

The $1/a$ value for the TCE/air system indicates that air will not displace TCE unless its pressure is 6.8 cm higher than the TCE pressure. For the TCE/water system, the pressure in the TCE must be at least 12.8 cm higher than in the water, before it will displace it.

Residual TCE saturations, measured at the end of the TCE/air and TCE/water experiments at a number of locations along the column, were on average 0.085 and 0.050, respectively. As was to be expected, the residual TCE-value is greater in the TCE/air system than in the TCE/water system.

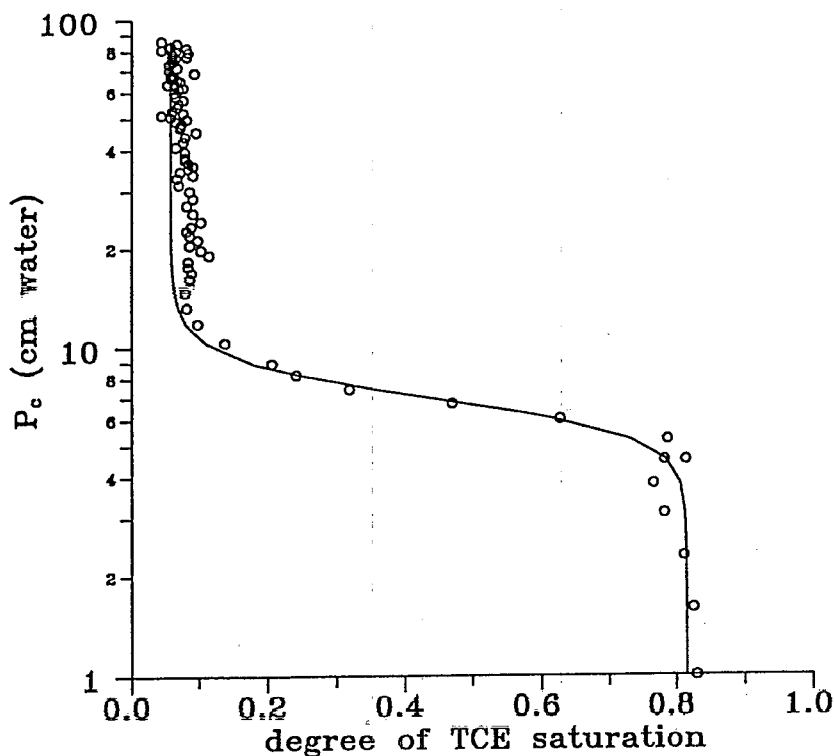


Figure 2. Capillary pressure (P_c) - saturation data during the displacement of TCE by air. The solid line represents the fitted van Genuchten curve ($a = 0.148$, $\eta = 7.244$, residual $S_{wr} = 0.059$, saturated $S_w = 0.817$).

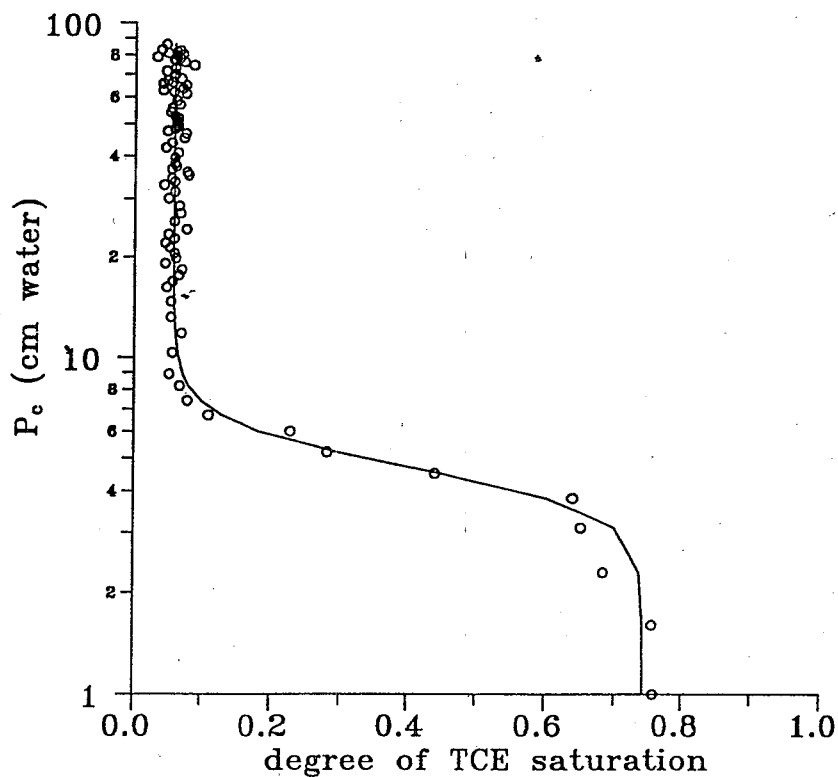


Figure 3. Capillary pressure (P_c) - saturation data during the displacement of air by TCE. The solid line represents the fitted van Genuchten curve ($a = 0.220$, $\eta = 6.657$, residual $S_{wr} = 0.059$, saturated $S_w = 0.742$).

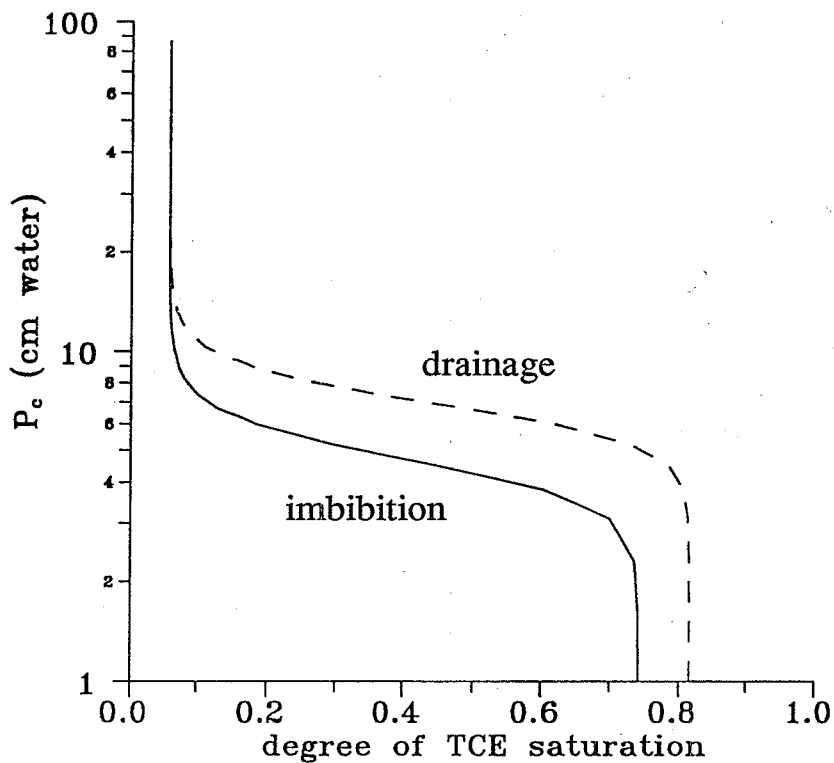


Figure 4. Capillary pressure (P_c) - saturation curves during drainage and imbibition of TCE for a TCE/air system.

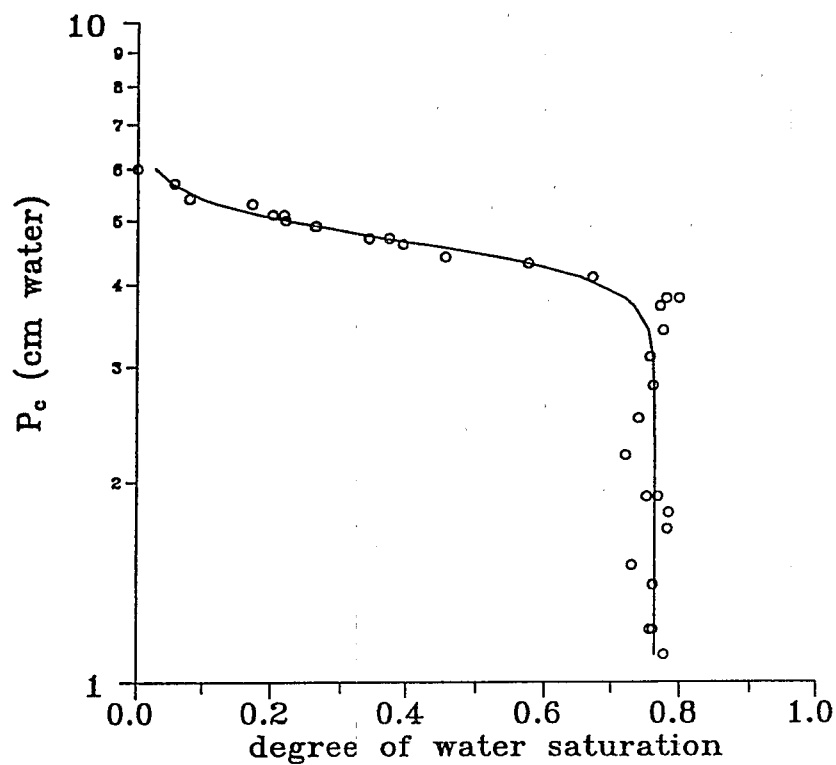


Figure 5. Capillary pressure (P_c) - saturation data during the displacement of TCE by water. The solid line represents the fitted van Genuchten curve ($a = 0.216$, $\eta = 13.752$, residual $S_{wr} = 0.0$, saturated $S_w = 0.763$).

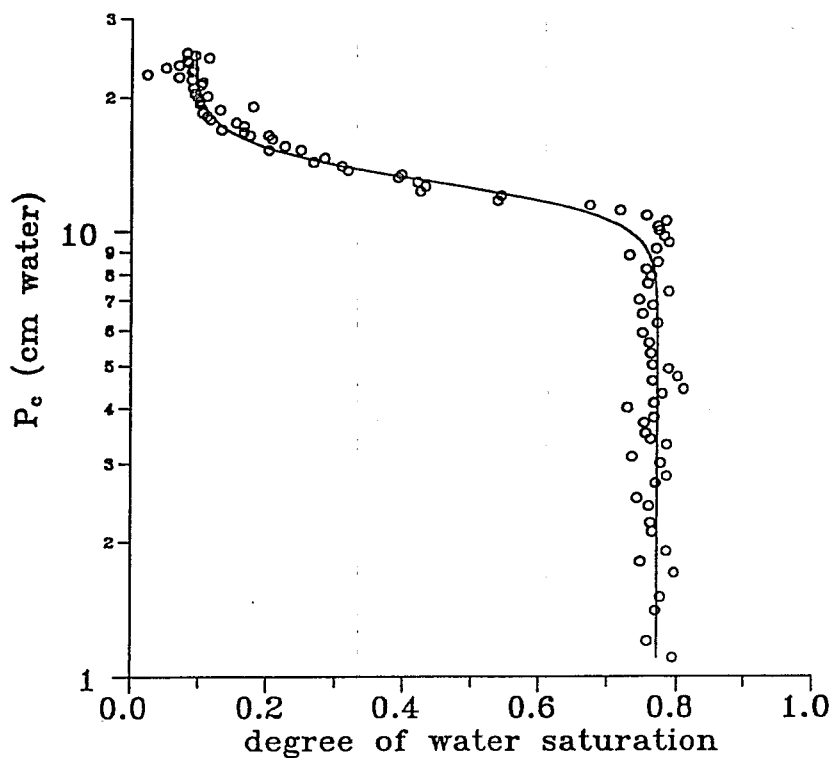


Figure 6. Capillary pressure (P_c) - saturation data during the displacement of water by TCE. The solid line represents the fitted van Genuchten curve ($a = 0.078$, $\eta = 10.457$, residual $S_{wr} = 0.093$, saturated $S_w = 0.770$).

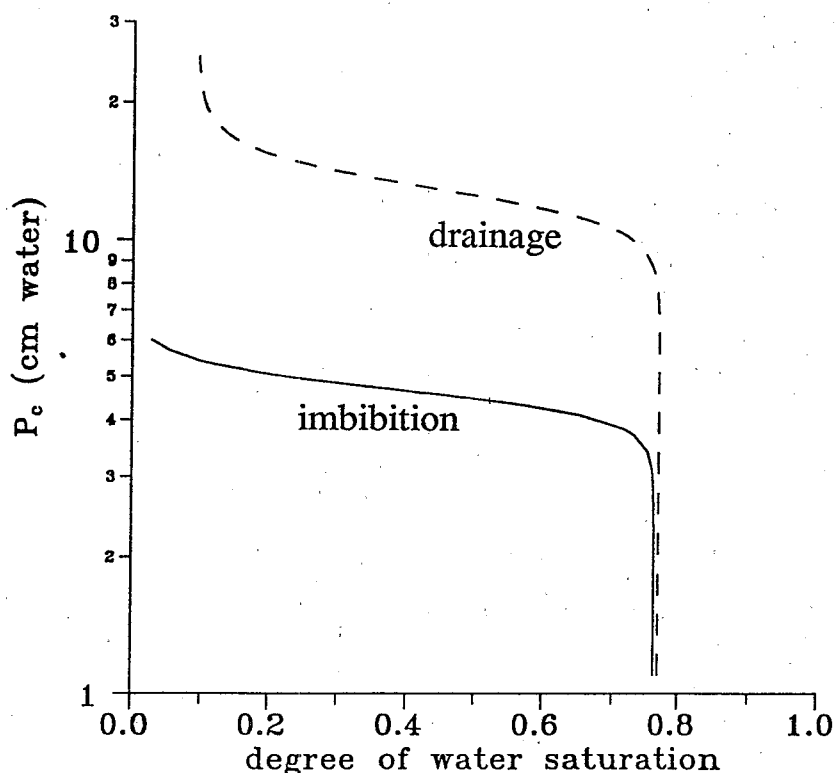


Figure 7. Capillary pressure (P_c) - saturation curves during imbibition and drainage of water for a TCE/water system.

Once a capillary pressure (P_c) - volumetric TCE content (θ_w), or saturation (S_w), curve has been determined from measurements taken at a point, as was done in this study (the collimated gamma radiation beam was 6 mm in diameter), the P_c - θ_w relationship can be calculated for a soil sample of a given height. As an example, we assumed a pressure cell with a 6 cm high sample, with cross sectional area A , initially saturated with TCE. The reference level for the gravitational head and the outlet of the pressure cell was taken at the midpoint of the sample. The P_c - θ_w relationship displayed in Figure 2 was chosen as the proper relationship for a point by point analysis. For given (assumed) air pressures applied to the pressure cell, we then calculated the P_c distribution in the soil sample: the TCE pressure (P^w) was computed at different vertical locations assuming a linear variation in P^w across the sample. Corresponding volumetric TCE values were taken from the curve in Figure 2. The average θ_w over the whole sample was then calculated by applying the trapezoidal rule. These average sample values are graphically displayed in Figure 8, together with some of the point measured data. It should be noted that the air entry value of the relationship determined by the gamma radiation system is clearly defined ($P_c = 5.4$ cm of water). The curve determined on a 6 cm high sample, however, starts to drain at the top when the applied air pressure is equal to 1 cm of water pressure ($P_c = 1$ at $z = 0$ and therefore $P_c = 5.4$ at $z = 3$). If the P_c - θ_w relationship had been determined on a 6 cm high sample, the air entry value would have been determined to be 1 cm of water pressure. Due to the early drainage of the top of the sample and the late drainage of the bottom part, the curve shows a much more gradual change in TCE content with P_c than

the one determined at a point. As a result substantial differences exist in θ_w for the same P_c .

Dissolution of Trichloroethylene at Residual Saturation in Groundwater

In many cases it appears that the mass transfer between the residual DNAPL and water is fast enough so that it can be assumed water leaving a region of residual saturation has dissolved concentrations of the DNAPL at the solubility limit. This is the typical assumption used in models for the transport of the dissolved organic species in the water phase. However, for nonuniform distributions of residual saturation, very small residual saturations, or high water velocities, the dissolution process might be mass-transfer limited. This part of this study focuses on the dynamics of the dissolution process in these situations for a particular chemical, trichloroethylene (TCE).

Dissolution Model

Dissolution of TCE at residual saturation in groundwater will be a function of many parameters including the water velocity, size and shape of the residual blobs or ganglia, temperature, and the effects of other chemical constituents and organic matter in the system. Perhaps the most problematic variable is the structure of the residual TCE ganglia.

To circumvent the problem of describing the interfacial area between the residual TCE and the water, we use a lumped-parameter model. At a particular location vector \vec{X} in a porous

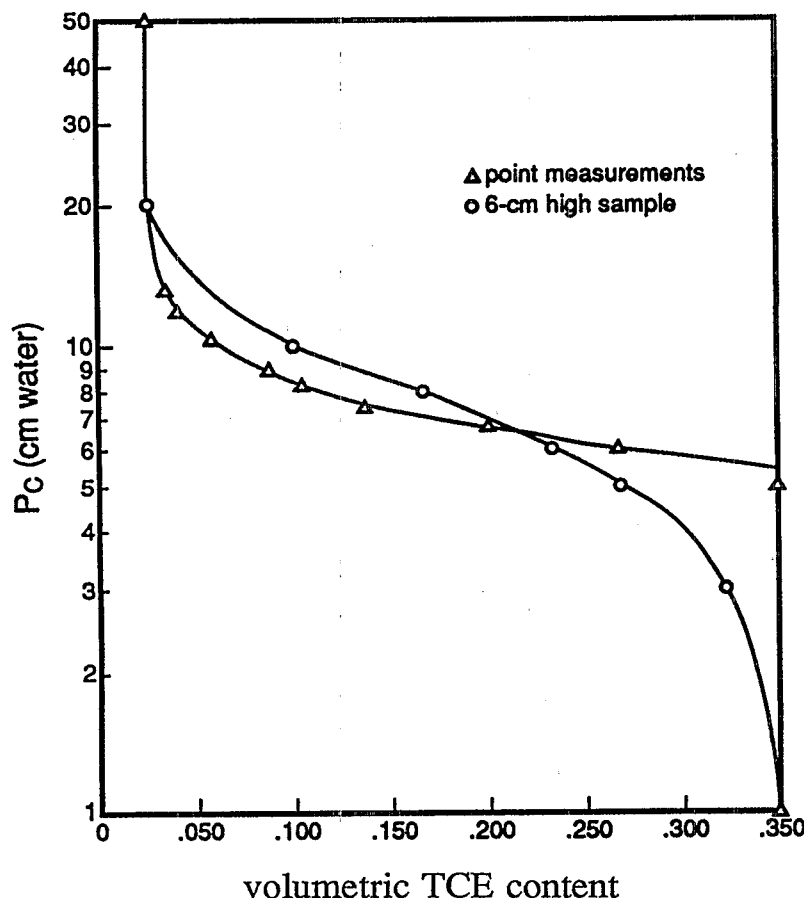


Figure 8. Capillary pressure (P_c) - volumetric TCE content (θ_w) during the displacement of TCE by air as measured at a single point (triangles) and as calculated for a 6 cm high sample (circles) from the data obtained at a single point.

matrix, the mass transfer for TCE is assumed to be described by:

$$\rho^n \epsilon(\vec{x}) \frac{\partial S_n}{\partial t} = C^{wn} [\rho_o^w(\vec{x}, t) - K_o^w] \quad (5)$$

where, as before, the superscripts denote phases [nonwetting (n) and wetting (w)] and subscripts denote species [TCE (o) and water (w)]. Implicit in this equation is a functional dependence of C^{wn} on the interfacial contact area between the water and TCE appropriate for some representative volume. We choose to express this functional dependence by developing a relation between C^{wn} and θ_n (TCE volumetric content, $\theta_n = S_n \times \epsilon$), where θ_n is now a representative measure of the interfacial contact area. Such a relation will likely be different for different pore structures and thus different porous media. C^{wn} will also vary with other system parameters including flow velocity and the presence of other chemical constituents and organic matter. In the work presented here, we discuss the relationship between C^{wn} and both θ_n and the water velocity for a particular sand.

To study the usefulness of this lumped-parameter model, we obtain local measures of ϵ and $\partial S_n / \partial t$ in a vertical sand column impregnated with TCE at residual saturation. The determination of ϵ and $\partial S_n / \partial t$ is facilitated by gamma attenuation which is

described below. The governing equation for the transport of dissolved TCE in the column is a simplified form of equation (1b):

$$\begin{aligned} & \frac{\partial}{\partial t} [\epsilon (1-S_n) \rho_o^w] + \epsilon (1-S_n) v^w \frac{\partial \rho_o^w}{\partial x} - \\ & \frac{\partial}{\partial x} [\epsilon (1-S_n) D^w \frac{\partial \rho_o^w}{\partial x}] = -\rho^n \epsilon \frac{\partial S_n}{\partial t} \end{aligned} \quad (6a)$$

where the hydrodynamic dispersion tensor is now a scalar quantity, D^w , and the term on the far right replaces the interface mass exchange term, ρ_o^w . An order of magnitude analysis and numerical studies suggest that for the experimental conditions encountered in this work all terms in equation (6a) are small except for the advection and interface mass exchange terms. In this case (6a) can be reduced to

$$\epsilon (1-S_n) v^w \frac{\partial \rho_o^w}{\partial x} = -\rho^n \epsilon \frac{\partial S_n}{\partial t} \quad (6b)$$

Since $\epsilon \partial S_n / \partial t$ can be measured quite accurately along the length of the column by gamma attenuation, equation (6b) is

integrated from the end of the column where $\rho_o^w(L, t)$ is measured to any desired location x . The resulting expression for $\rho_o^w(x, t)$ when substituted into equation (5) yields

$$C^{wn}(x, t) = \rho^n \varepsilon \frac{\partial S_n}{\partial t} \left[\frac{1}{\rho_o^w(L, t) + \frac{\rho^n}{\varepsilon(1-S_n)^{vw}} \int_x^L \varepsilon \frac{\partial S_n}{\partial t} dx' - K_o^w} \right] \quad (7)$$

Thus, $C^{wn}(x, t)$ is a function of parameters measured experimentally: $\varepsilon(x)$, $\rho_o^w(L, t)$, and $\partial S_n / \partial t(x, t)$.

Experimental Method

Five different experiments were run at Darcy velocities ranging from 0.1 to 1.4 m/day while maintaining a constant room temperature of $21.5^\circ\text{C} \pm 1.0^\circ\text{C}$. The Darcy velocity remained essentially constant throughout each experiment. Concentrations of TCE in the column effluent were measured in each of the experiments by extracting 200 μl water samples into 500 μl of methanol. At each sampling time, three such samples were collected and then analyzed by injecting 1 μl of the mixture into a gas chromatograph equipped with a flame ionization detector.

S_n and ε were measured along the column by gamma attenuation. The primary system components are a gamma radiation source, 450 mCi of ^{241}Am , and a NaI (TI) scintillation detector, each mounted securely on a movable platform. The sample cell is fixed between the source and detector; and with the collimation of the radiation beam, a 1 mm thick horizontal slice containing 48% of the cross-sectional column area can be scanned. The remainder of the system is described by Ferrand, et al. (1986). The system here is exactly the same as theirs except that the ^{137}Cs source contained in their system was removed, allowing for more accurate measurements.

Of primary importance is to achieve accurate measures of the porosity and TCE saturation. Average values of both measures are determined for each 1 mm horizontal slice of the column which is irradiated. For the particular calibration and measurement schemes developed for our work, we find the following theoretical estimates for the errors in these measures:

Parameter	Bound for Systematic Error	Random Error (One Estimated Standard Deviation)
ε^k	± 0.003	---
S_n^k	± 0.008	± 0.002 to ± 0.004

The superscript k denotes the value of the parameter measured in a particular horizontal slice k which has been irradiated. The ranges given for the random error in S_n^k are indicative of the errors expected over the range of counting times used with the gamma radiation system in the five experiments. Note that

since ε^k is measured once at the beginning of the experiment, any error in its value will appear as a systematic error in subsequent analyses.

A very uniform quartz sand with grain diameters ranging between 0.30 mm and 0.42 mm was used. This sand was washed and incinerated to remove any fines and organic matter. The oven-dry sand was packed tightly in an aluminum cell 8.25 cm in diameter and 3 cm deep on top of a perforated stainless steel plate covered by a Teflon mesh screen with 0.149 mm openings. Typical porosities obtained were between 0.34 and 0.37. A 0.5 bar ceramic plate was placed on the sand surface and supported from above so that the sand column was in compression. An O-ring provide a seal between the walls of the aluminum cell and the ceramic, and a glass fiber filter disk was inserted between the sand and ceramic plate to enhance the hydraulic contact between the ceramic and the sand.

The column was gently flushed first with CO_2 and then with deaired deionized water from below, leaving the porous media saturated with water. TCE was then carefully added from below until a head of 62.5 cm (± 1 cm) of water was established across the ceramic plate. At this point, the TCE was typically at a saturation of $\approx 80\%$ throughout the column. To displace the mobile TCE, two pore volumes of water were pumped through the column from above at the Darcy flow rate chosen for the experiment. At the completion of this flush, a complete scan of the column was made to measure the residual TCE saturation (S_{nr}) for each 1 mm horizontal slice of the porous media. Over the entire five experiments, values of S_{nr} for these 1 mm thick sections ranged between 10-19%, with S_{nr} typically between 11-14%. The dissolution experiment was then started by resuming the flow of water and initiating both the gamma radiation and effluent concentration measurements. The gamma radiation system, mounted on a movable platform, automatically scanned the column at 1 mm vertical intervals continuously, pausing at each location to collect data. Water samples were removed intermittently from the column effluent for analysis of TCE concentrations. The experiment was stopped when there was no detectable TCE in the column from the gamma radiation measurements.

A comparison between the gamma attenuation measurements and measurements of TCE concentrations in the effluent water provides a mass balance check. For each experiment the mass of TCE leaving the column in the water phase was greater than the mass measured with gamma attenuation. This error ranged between 12-38% for the five experiments. Evidence from a test independent of these experiments indicates that during the initial TCE invasion of the porous media, a significant mass of TCE could leak around the O-ring sealing the ceramic plate against the sand at the top of the column. This extra TCE cannot be measured with gamma attenuation, and is the likely cause of these mass balance errors. The computed C^{wn} are not affected by these errors, since they are based on local measures of $\partial S_n / \partial t$ and ρ_o^w . [Values of $\partial S_n / \partial t$ are measured directly with gamma attenuation. $\rho_o^w(x, t)$ are computed by integrating $(\rho^n \partial S_n / \partial t) / v^w (1 - S_n)$ from each x to the end of the column ($x = L$) and adding this to the measured $\rho_o^w(L, t)$. Equation (7) shows this computation.] Further details of the experimental techniques and a discussion of these errors can be found in Imhoff, et al. (1992).

Results

The results can best be illustrated by first examining one experiment in detail. Here, we will look at the experiment where a Darcy velocity of 0.53 m/day was used. A plot of the changing TCE saturation along the column is shown in Figure 9. As clean water enters from the top, TCE is dissolved in this region and the TCE saturation decreases. Once the TCE saturation reaches essentially zero at the very top of the column, a dissolution front of length X^* has formed. Although it is difficult to observe in this figure, this dissolution front moves downward through the column, remaining essentially the same length. After about 200 pore volumes, essentially all of the TCE entrapped in the column is dissolved away.

Figure 10 shows the changing TCE saturation versus time for the location 3 mm from the bottom of the column (shown in Figure 9 with a square around the data). Until the dissolution front reached this location, there was no measurable TCE transport due to mobilization of the residual ganglia. Also, there is no increase in the slope of the data for small saturations which might indicate mobilization of dissolving ganglia. A seventh degree polynomial was fit through the S_n -t data and $\partial S_n / \partial t$ was

found by taking the derivative of this polynomial. The use of such a high degree polynomial allowed for an accurate fit to the curvature exhibited by the data at very high and low S_n . Such curvature is not significant in Figure 9, but is more pronounced for other column locations. Similar analyses were performed on the data collected at these other locations.

Figure 11 shows the computed C^{wn} versus changing θ for all column locations. The different data symbols indicate data taken from different column locations, where some repetition of the symbols was necessary to plot all data. The outliers come largely from data locations near the very top and bottom of the column where it was more difficult to obtain accurate measures of θ . In the region of the column where the dissolution front forms ($x \leq X^*$), for a given θ , the numerical value of C^{wn} decreases as one moves down in the column. Once the dissolution front is formed ($x \geq X^*$), the C^{wn} versus S_n relation remains essentially invariant with column location. This same general trend was observed in the other experiments, and it is discussed in detail in Imhoff, et al. (1992). It is believed that the most accurate data are from the region ($x \geq X^*$), and these data were used in all subsequent analyses.

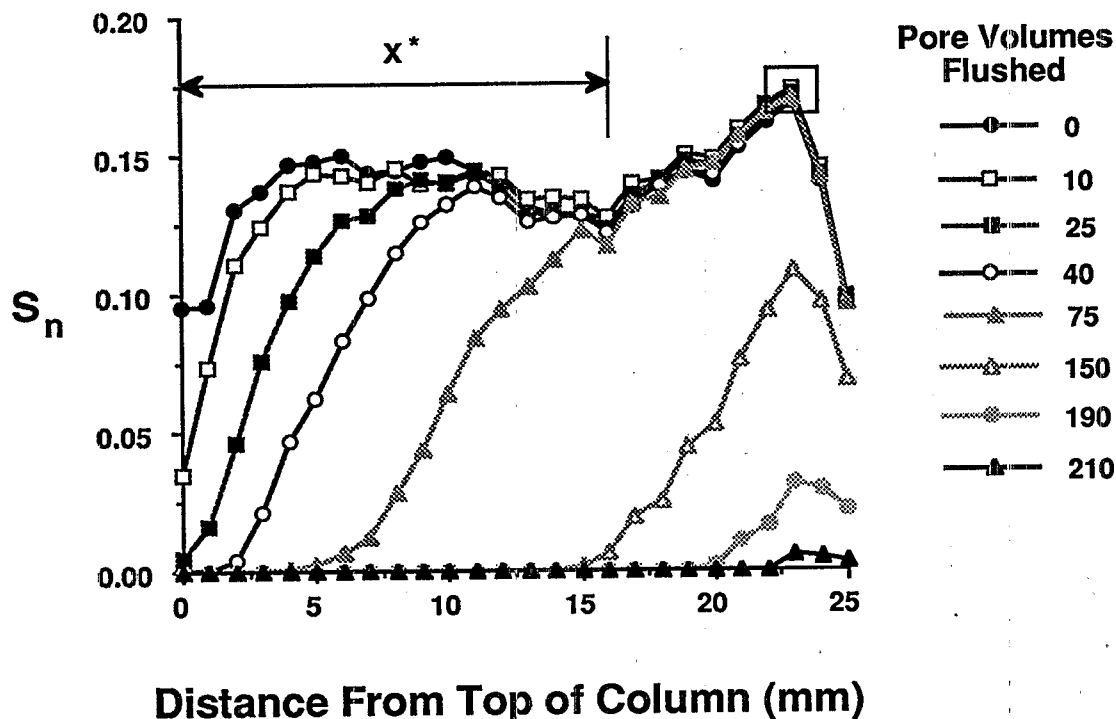


Figure 9. Changing profile of TCE saturation, S_n , during experiment. Darcy velocity = 0.53 m/day. See text for further explanation.

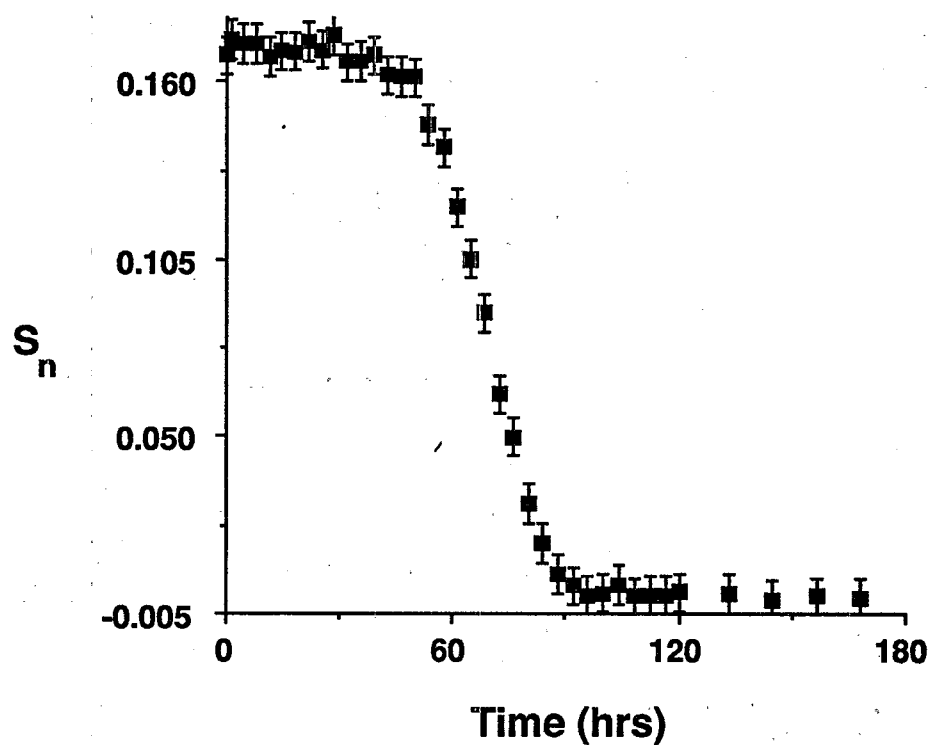


Figure 10. Changing TCE saturation, S_n , versus time for location 3 mm from bottom of the column. Darcy velocity = 0.53 m/day. Error bars represent \pm one estimated standard deviation.

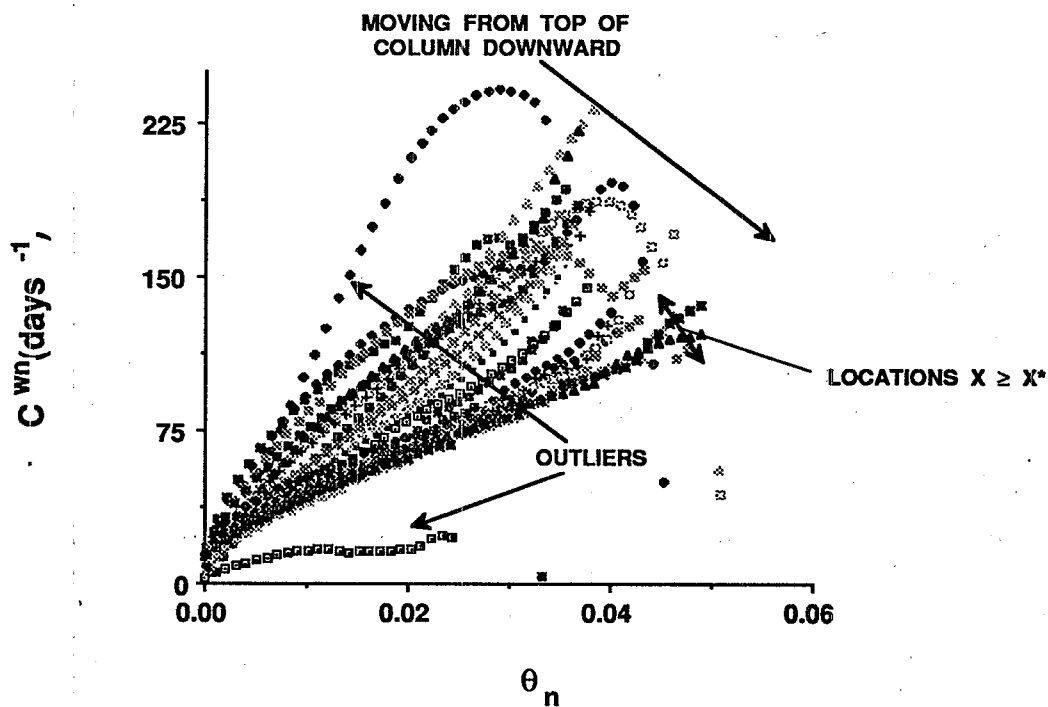


Figure 11. Changing mass transfer rate coefficient, C^{wn} , with TCE volumetric content, θ_n , for all column locations. Darcy velocity = 0.53 m/day.

The trend of decreasing C^{wn} with decreasing θ_n is primarily due to the changing contact area between the water and TCE phases. Thus, as θ_n decreases the contact area decreases and the mass transfer process slows.

The data from all experiments were put in dimensionless form using the following parameters:

$$\theta_n = S_n \varepsilon$$

$$Sh = \frac{C^{wn} (d^p)^2}{D_o^w}$$

$$Sc = \frac{\mu^w}{\rho^w D_o^w}$$

$$Re = \frac{v^w \rho^w d^p}{\mu^w}$$

where θ_n is the TCE volumetric content, Sh is the Sherwood number (the ratio of the mass transfer velocity to the diffusion velocity), Sc is the Schmidt number (the ratio of the diffusivity of momentum to the diffusivity of mass), and Re is the Reynolds number (the ratio of inertial forces to viscous forces) (Cussler, 1984). The new terms in these expressions are d^p = mean grain

diameter [L], and D_o^w = molecular diffusivity of TCE in water [L^2/T].

Sh is plotted versus Re for three representative values of θ_n in Figure 12. The vertical bars indicate the range of data collected for all $x \geq X^*$ at each Re . For a constant value of θ_n , as Re increases Sh increases in an approximately linear fashion up to $Re \approx 0.01$. Thus, as the interstitial water velocity increases, C^{wn} increases although there appears to be some limit to this effect. The increase in C^{wn} with Re for $Re \leq 0.01$ is likely due to a thinning of the diffusion zone between the surface of residual TCE phase and the bulk water. This effect is illustrated in Figure 13, where as Re increases, the thickness of the stagnant film (or diffusion zone) decreases, i.e., l becomes smaller in Figure 13.

A second trend is the increase in C^{wn} with θ_n , which was noted above for Darcy velocity = 0.53 m/day. Here, this same trend is seen for all Re , indicating that the interfacial contact area increases as θ_n increases.

The data were fit to a power-law model of the same form as Miller, et al. (1990) using least squares regression:

$$Sh = \beta_1 \theta_n^{\beta_2} Re^{\beta_3} Sc^{1/2} \quad (8)$$

$$\beta_1 = 3.18$$

$$\beta_2 = 0.54$$

$$\beta_3 = 0.98$$

The coefficient of multiple determination (r^2) = 0.94. The fitted parameters are best estimates; confidence intervals could not

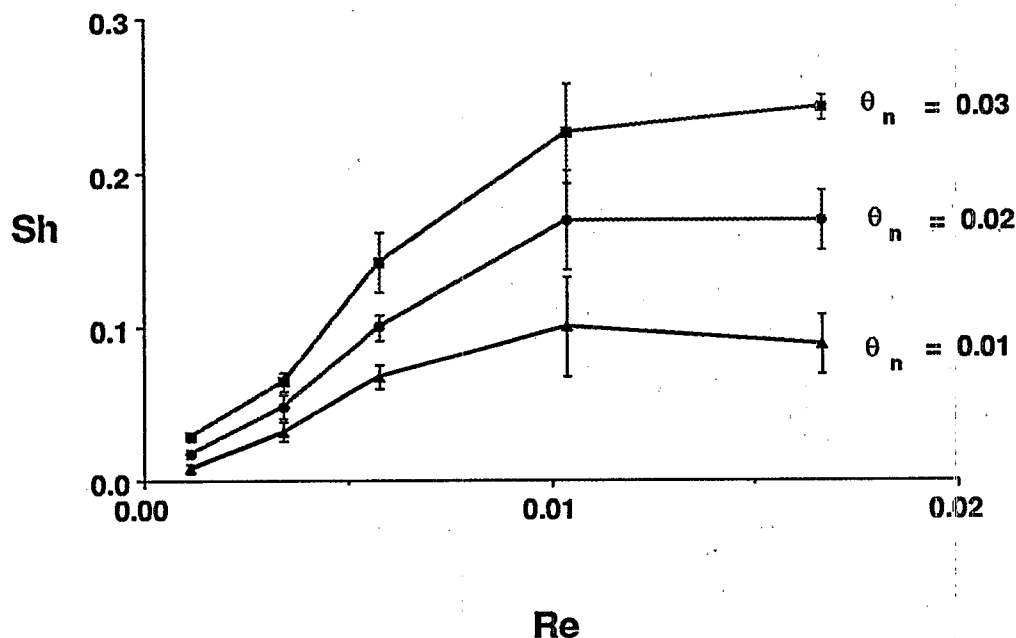


Figure 12. Sherwood number, Sh , versus Reynolds number, Re , for three values of TCE volumetric content θ_n . Vertical bars represent the range of data collected for all column locations.

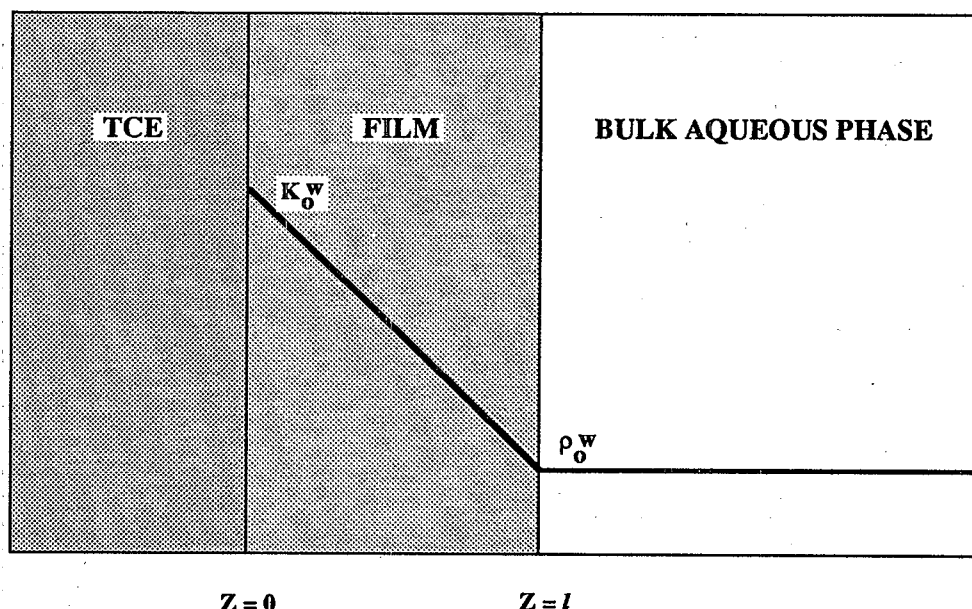


Figure 13. Stagnant film model for mass transfer. The interfacial region is idealized as a hypothetical film which is unstirred. Mass transfer involves diffusion across this film from pure TCE to the bulk aqueous phase. K_o^w is the solubility limit of TCE in water ρ_o^w is the concentration of TCE in the bulk water.

be determined for these parameters since an analysis of the residuals from this model indicates the model errors are correlated (Imhoff, et al., 1992).

The Schmidt number was included in this model for comparison with the work of Miller, et al. (1990); as with this work, only θ and Re were varied in their study. The best estimates for the fitted parameters determined by Miller, et al. (1990) were: $\beta_1 = 12 \pm 2$, $\beta_2 = 0.60 \pm 0.21$, and $\beta_3 = 0.75 \pm 0.08$, where the range specified for each parameter represents a 95% confidence interval. There is good agreement for the value of β_2 , but appreciable differences for the other parameters. These differences may be explained by several factors: Miller, et al. (1990) used a glass bead media and a different technique for establishing the initial residual TCE (S_n); measured dissolution for discrete S_n (and not as S_n slowly decreased with time as here); and used toluene as the dissolving NAPL rather than TCE (different contact angles may result for the different NAPLs yielding different interfacial areas for mass transfer for the same S_n). In addition, the variation of C^{wn} with location along the sample column was observed in this study but remains unexplained. Miller, et al. (1990) were not able to measure variations of C^{wn} along their sample columns. These issues are explored in detail in Imhoff, et al. (1992). However, additional experimental work using both different porous media and NAPLs with different contact angles is required to fully address these issues. Thus, the mass transfer model developed in this study is valid only for this porous media and TCE.

Importance of Nonequilibrium Dissolution

Given the added complexity in incorporating a mass transfer model in a numerical simulation of NAPL transport, it is reasonable to investigate the conditions for which this is

necessary. The experimental work described above provides insight into this question. In these experiments, mass transfer was sufficiently fast so that even after the formation of a dissolution front (see Figure 9), aqueous phase TCE concentrations reached the solubility limit over distances of less than 3 cm for Darcy velocities between 0.1-1.4 m/day. S_n ranged from $\approx 0\%$ to 10-19% over these dissolution fronts. Clearly, if conditions similar to these occur in nature, modeling nonequilibrium dissolution for the prediction of aqueous phase TCE concentrations will be unnecessary. However, if instead the objective is to capture the dynamics of the changing TCE saturation, then use of the local equilibrium assumption will give very different results. Local equilibrium between the water and TCE phases would require the complete removal of TCE from an element in a numerical simulator before dissolution could begin in the adjacent downstream element. Thus, use of the local equilibrium assumption would not predict the formation of the dissolution front illustrated in Figure 9.

Even if interest is limited to the prediction of aqueous phase TCE concentrations, modeling nonequilibrium dissolution could be important for many real-world situations. Two cases for which the situation would be different from that considered in these experiments are: (1) TCE ganglia of similar size and shape but distributed nonuniformly in the porous media, and (2) TCE ganglia uniformly distributed throughout the media but varying widely in size and shape. The numerical model described below can be used to investigate the importance of modeling nonequilibrium dissolution for case (1). Various distributions of residual TCE could be created in a hypothetical aquifer modeled with the two-dimensional simulator. By using the nonequilibrium dissolution model in this simulator, downstream TCE concentrations can be predicted. Comparing these with those generated from the same simulator but which assumes local

equilibrium between the TCE and water will provide information on the importance of modeling nonequilibrium dissolution.

Case (2) is more difficult to analyze. In this study, the use of a very uniform sand likely created TCE ganglia of similar size and shape throughout the media. A natural aquifer will often contain lenses of coarse and fine material. Wilson, et al. (1990), using micromodels, show how a large NAPL ganglion can be isolated in a coarse lens embedded in such media. Since the interfacial contact area per unit NAPL volume decreases with increasing ganglion size, mass transfer can be expected to also decrease for the larger NAPL ganglia in this media. Although the form of the dissolution model developed from our experimental study should be correct for this case, the parameters may be different.

Thus, while this experimental study provides important information on the dissolution of TCE in the saturated zone, more work is required to elucidate those situations where it is important to model nonequilibrium dissolution for the prediction of aqueous phase TCE concentrations.

Numerical Methods and Model Development

Coupled with the experimental investigations, numerical methods were developed to solve the equations that describe two-phase flow in porous media with associated dissolved transport and mass exchange. The approach taken included fundamental developments and analysis, as well as construction of a practical two-dimensional, two-phase simulator that includes mass exchange and miscible transport in the aqueous phase. Standard approximation methods, including finite difference and finite element methods, were investigated and analyzed in the context of multiphase flow simulation. From this came a set of recommendations for use of these approximations. Matrix solution techniques were also investigated, as were methods for solution of the miscible transport equations. This work is summarized below, and the numerical algorithm implemented to solve the full immiscible/miscible problem is described.

To begin, a complete analysis of the model multiphase equation, Richards equation, was undertaken. After extensive investigation of solutions using finite difference and finite element methods, the following conclusions were drawn: (1) Mass balance problems must be adequately controlled in these types of equations. Thus the mass-conservative approximation referred to as the Modified Picard method was recommended. (2) In finite element approximations, mass lumping is necessary to eliminate oscillations that occur ahead of steep moisture fronts. Thus a lumped finite element approximation, using a Modified Picard linearization, was recommended. Details of these results may be found in the paper of Celia et al. (1990a).

Based on these results, a formulation for the two-phase case was developed. Details of the numerical formulation are provided in Celia and Binning (1992). This algorithm was used to examine the movement of air in unsaturated soils under infiltration. From solution of the two-phase equations, it was observed that even though Richards equation is often a good approximation for the liquid movement, the motion of the air phase is still an important factor for contaminant transport in the air phase. That is, while the motion of the air does not affect significantly the motion of the water, it can have important

implications for transport of volatile contaminants in the unsaturated zone. Figure 14 illustrates a transient infiltration front with associated pathlines for particles of air. Notice that the air above the wetting front is flowing upward, toward the land surface, while that ahead of the front is moving downward. As the front progresses downward, air at progressively larger depths is pushed upward. This bifurcated flow seems to be characteristic of the air phase in unsaturated soils.

One of the outstanding problems in multi-dimensional numerical simulations for multiphase flow and transport systems is the matrix solution step. Because the set of flow equations usually leads to symmetric matrices, a variety of iterative solvers can be applied with confidence. The paper of Bouloutas and Celia (1991) describes an efficient conjugate gradient algorithm for these equations. However, when solving the miscible transport portion of the problem, the matrices are inherently unsymmetric; and matrix solution becomes a more difficult issue. One possible approach is to employ a method that symmetrizes the resulting matrix. The Eulerian-Lagrangian Localized Adjoint Method (ELLAM) of Celia et al. (1990b) is one possible choice. This has the advantage of also providing enhanced accuracy due to the Lagrangian approach to advection and also possesses demonstrable mass conservation properties. This method has been developed extensively for one-dimensional systems (Celia and Zisman, 1990), but the two-dimensional implementation is not yet completed.

A second avenue for efficient matrix solution involves approximate factorization techniques. These include operator factorization or alternating-direction (AD) methods and iterative relaxation matrix factorization (for example block successive relaxation). A major motivation for development of these schemes is to reduce the solution of one large problem to a series of solutions of smaller independent subproblems which can be computed in parallel. One example of AD methods is the AD collocation (ADC) method of Celia et al., (1987) and Celia and Pinder (1990). In addition to being highly parallelizable, because the ADC method has collocation as its basis, it provides the added benefit of continuous velocity fields from pressure solutions on rectangular grids. This is convenient when solving miscible transport equations coupled to the flow (phase) equations. However, because this method employs operator factorization, it cannot directly accommodate cross derivative tensorial terms inherent in the governing equations. Therefore, a collocation based matrix factorization algorithm has been developed for the two-phase flow and transport equations described above. Because this is the algorithm employed in the computer code delivered to the EPA, a more detailed description is provided below.

Collocation Discretization/Linearization

Equations (1a) are rewritten in terms of the dependent variables, S_w and P^w , by noting that the phase saturations sum to unity, $S_w + S_n = 1$, by substituting the multiphase extension of Darcy's law, equation (2) into equation (1a), and by relating S_w to the capillary pressure, $P_c(S_w) = P^n - P^w$, when both phases are mobile, e.g., $\nabla P^n = [\nabla P^w + (dP_c/dS_w)\nabla S_w]$ (see for example Aziz and Settari, 1979, pages 133-134). Equations (1b) are written in terms of the dependent variable mass concentration, P_i^a .

Water Content vs. Time

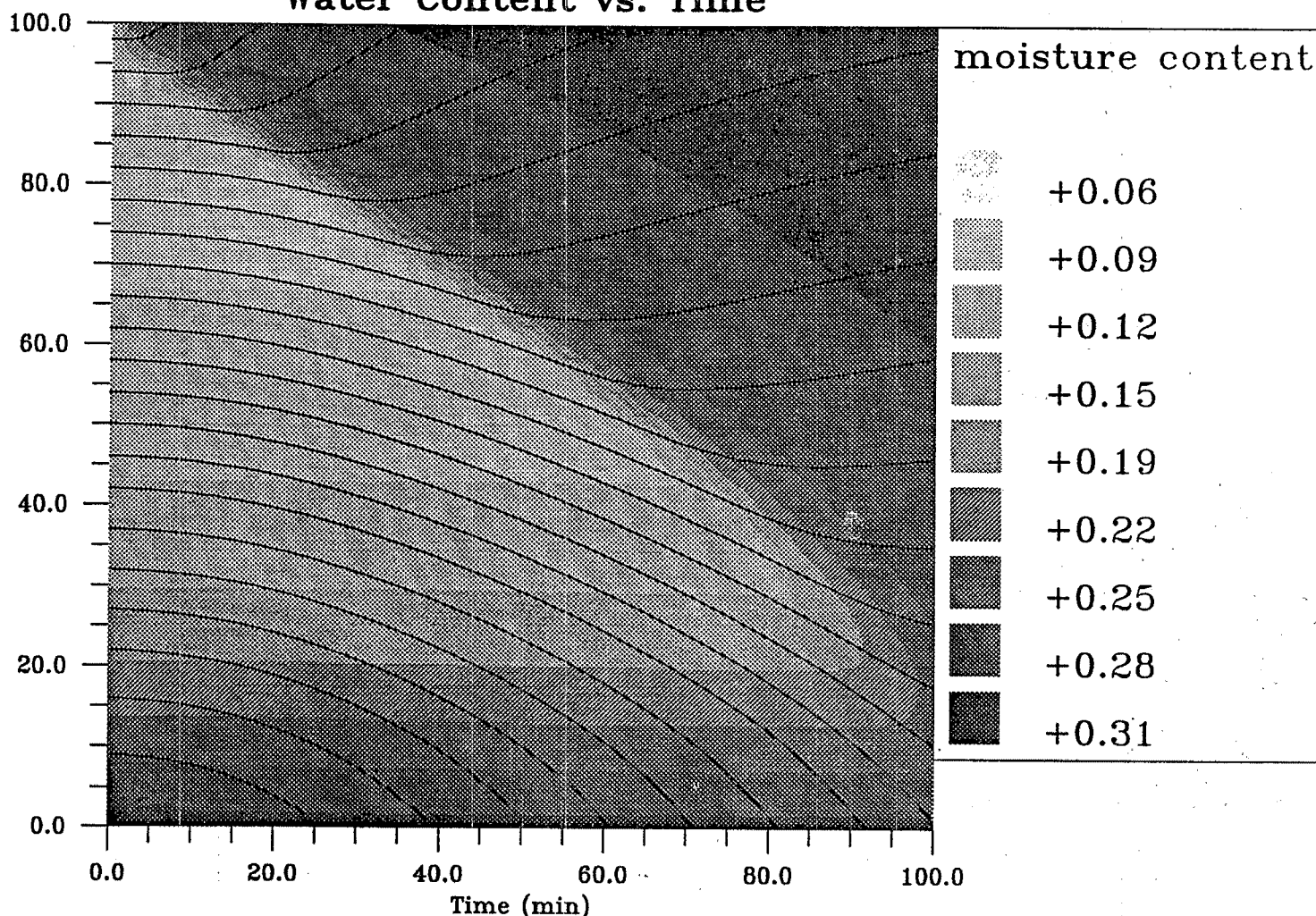


Figure 14. Infiltration of water into a column of porous material that is initially filled with air and water. Each vertical slice of the figure represents the state of the column at a particular time. The gray shading indicates the moisture content. The lines show the path of particles of air as the water infiltrates into the column.

The dependent variables, S_w , P^w and p_i^α , are approximated in space using a linear combination of bicubic Hermite polynomial basis functions. For two-dimensional problems this results in four degrees of freedom at each node for each variable (the function, the two first order derivatives and cross derivative). The other variables which are space dependent are approximated using bilinear Lagrange basis functions. The nonlinear terms, ρ^α , $k_{\alpha\alpha}$ and (dP/dS_α) in equations (1a) and $S_{\alpha\alpha}$, v^α and D^α in equations (1b), are evaluated at the node and interpolated into the element using bilinear Lagrange basis functions. Because the mass exchange term, \hat{p}_i^α , represents the main coupling between the flow and transport equations (a function of all the dependent variables), it is evaluated using hermite interpolated dependent variables.

Equations (1) are discretized in time using an implicit backward differencing scheme. The equations are linearized by the typically robust and relatively simple to implement Picard iteration technique, wherein the functions of the dependent variables are dated at the known iteration level and successively updated (see for example Huyakorn and Pinder, 1983).

The discretized equations are reduced to a set of linear algebraic equations by employing the orthogonal collocation method: a method of weighted residuals wherein the weighting function is the Dirac delta function. This is equivalent to driving the residual to zero at specified points in the domain which are denoted as collocation points. Thus no formal integrations are required; and generation of the system matrix is computationally

analogous to the finite difference method. Orthogonal collocation results when the equations are written at the four gauss quadrature points in each element.

System Matrix Generation/Solution

Equations (1) define the nonlinear relationship between phase flow and constituent transport. In general, the flow equations (1a) define the distribution of the phases given phase composition; while the transport equations (1b) define the phase composition given phase distribution and velocity fields. While rigorous evaluation of this system of four equations would require a simultaneous iterative numerical technique, if we note that the flow and transport equations are only weakly coupled through the phase density, viscosity and exchange terms, a less computationally intensive way to solve the system is to decouple the equations. This so called *decoupled approach* has been used in the modelling of saltwater intrusion problems [Celia and Pinder, 1990] and has been applied to multiphase flow and multicomponent transport problems by Reeves and Abriola (1988). The decoupled approach can be summarized as follows:

1. Given the most recent solution to the transport equations (1b), the phase flow equations (1a) are in general solved simultaneously for P^w and S_w (see for example Aziz and Settari, 1979, pages 133-134). The transition between two-phase flow and one-phase flow (DNAPL at residual) is incorporated by forcing k_r

to go to zero faster than dP/dS_w goes to infinity. In those portions of the domain where DNAPL is absent only the water phase balance equation (1a) is solved for P^w .

2. Given the flow solution which defines the phase distribution and velocity field, solve the uncoupled, weakly nonlinear, transport equations (1b) for p_o^w and P_w^n .
3. Recalculate the flow equations with the new composition distribution. Update composition using the new flow solution. Repeat until changes are small in some appropriate norm.

This approach allows for smaller systems of equations to be solved at any one time, allows concurrent execution of each constituent transport equation, and allows for the incorporation of additional constituents with little restructuring of the solution algorithm.

The system matrices created by using the above discretizations are tri-diagonal (this results from the collocation numbering scheme; see for example Lapidus and Pinder, 1982, pages 337 and 338). During each iteration on the nonlinearities, spatial decoupling is approximated by using a relaxation matrix splitting scheme wherein the main diagonal blocks are treated implicitly and the off diagonal blocks are treated explicitly. This results in an approximate solution to the system of equations over each nonlinear iteration. The effect of the relaxation scheme is to reduce the solution to a series of independent subproblems or sweeps which can be computed in parallel. For a more detailed explanation of the parallel solution algorithm see Eppstein et al. (1992) and Guarnaccia (1992).

Numerical Treatment of Dissolution

A final consideration in the solution algorithm is how dissolution of residual organic is incorporated into the model. Two major issues must be addressed. First is the emplacement of the residual which requires treatment of hysteresis in $S_w(P_c)$. The hysteresis algorithm used in the simulator is based on the hysteretic K-S-P models proposed by Kool and Parker (1987) and Luckner et al. (1989). Specifically, the K-S-P model presented in equations (4) is augmented to include hysteresis by defining drainage and imbibition curves based on case-specific parameter sets. The result is that water imbibition curves generally terminate at $S_w < 1$, where by definition $k_r = 0$. In these cases, the phase mass balance equation for the NAPL reduces to a balance between a change in saturation and the dissolution rate term. Details of the hysteresis algorithm can be found in Guarnaccia and Pinder (1992).

The second major issue is the incorporation of the mass exchange term. The model uses equation (3) with C^{wn} defined by equation (8). To force the model to assume local equilibrium between the NAPL and water phases, the parameter β , in equation (8) would be increased to a very high value.

Model Verification

The flow portion of the code was verified by comparing numerical results with the exact integral solutions of McWhorter and

Sunada (1990) for two-phase flow. The integral solutions provide comparison for various horizontal, immiscible phase displacement scenarios in the presence of capillary pressure. The K-S-P model utilized was the van Genuchten model (equation 4). Figure 15 shows a close agreement between the integral and the numeric solutions for a unidirectional displacement of a wetting phase by a nonwetting phase. The fluid and soil properties for this problem are: viscosity ratio = 2.0, $S_{wr} = 0.05$, $\alpha = 0.098 \text{ cm}^{-1}$, $\eta = 2.5$, $\epsilon = 0.1$, $k = 5.0 \times 10^{-7} \text{ cm}^2$; the initial condition is $S_w(x, 0) = 1.0$; and boundary conditions are: inflow boundary - $S_w(0, t) = 0.6$, outflow boundary - $S_w(100, t) = 1.0$.

The mass exchange/transport portion of the code was verified by numerically simulating the dissolution experiment described above and illustrated in Figure 9. The experiment was designed to study the dissolution of residual TCE in a uniform sand column by flushing the system with clean water and tracking the dissolution front as a function of time. The input parameters used in the numerical model follow.

The initial conditions for residual TCE saturation are provided in Figure 16 ($t = 0 \text{ PV}$). The initial conditions on the dissolved TCE species were set at the solubility limit. The mass transfer rate coefficient was obtained from equation (7). A spatially variable porosity (average 0.35) was used, based on gamma attenuation measurements. Other physical parameters were obtained from the literature at the temperature at which the experiment was performed. The one-dimensional system was modelled as a strip of elements with no flow boundaries on the vertical sides and uniform conditions along horizontal boundaries. The top horizontal boundary had Dirichlet conditions specified on both water pressure (homogeneous) and the dissolved TCE species (time varying decay in concentration). The bottom horizontal boundary had Neumann conditions specified on both water pressure (such that the Darcy velocity was 0.53 m/day) and on the dissolved TCE species (homogeneous). The model length was 25 mm and the spatial discretization used was 1 mm. The simulation time was 100 hours and the time discretization used was 100 seconds.

Figure 16 shows a plot of the saturation profiles of the experimental and the numerical results for times in pore volumes (PV) of 50, 100 and 180 PV. The match in simulation results was excellent from an engineering point of view. Note the close agreement in terms of mass balance. The results predict complete TCE removal in less than 100 hours or about 200 pore volumes of water flushed. However, it is apparent that C^{wn} is generally too low to capture the precise shape of the experimental fronts. The discrepancy is probably due to two basic sources of error: first, equation (7) was fit to data from five separate experiments and we are attempting to reproduce only one of these five; and second, it was fit to data in the lower portion of the column.

Summary and Conclusions

An efficient collocation based numerical algorithm designed to solve nonlinear multiphase flow and multicomponent transport problems in porous media has been described. Specifically, the target problem is the description of the emplacement and subsequent removal through dissolution of contaminant NAPLs in near-surface saturated groundwater environments. The

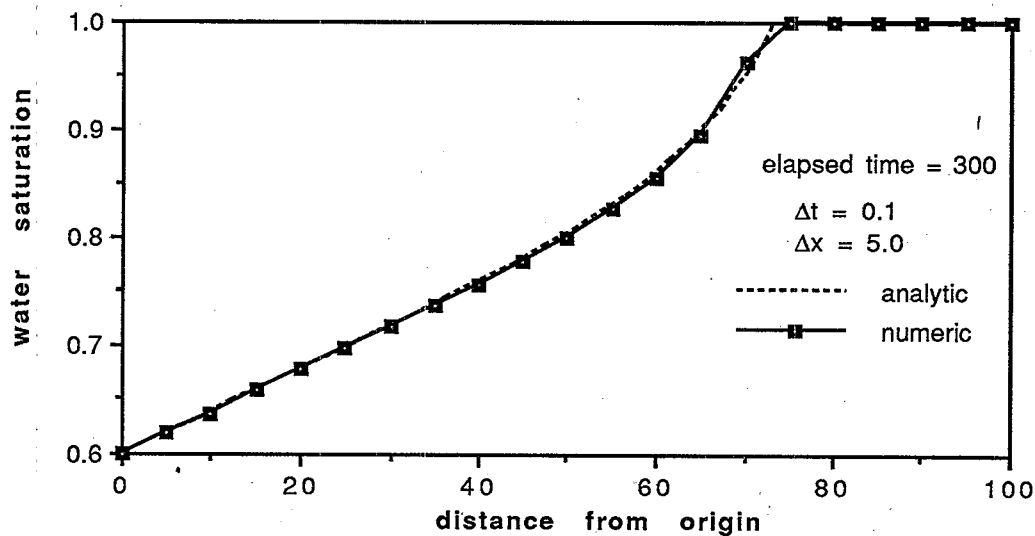


Figure 15. Unidirectional displacement of a wetting phase by a nonwetting phase: comparison between the analytical solution of McWhorter and Sunada (1990) and the numerically simulated solution.

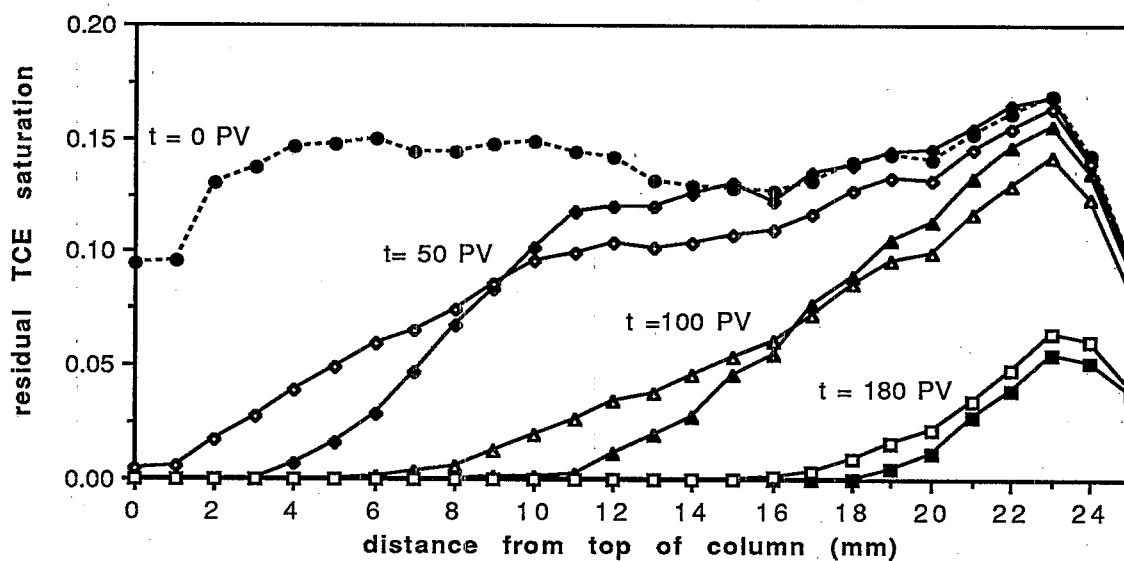


Figure 16. Comparison between experimental (black symbols) and numerical results (white symbols) for a dissolution experiment where residual TCE was removed from a column by flushing it with clean water. This figure uses the same data as that presented in Figure 9.

method is relatively simple to implement and exploits parallel execution to dramatically reduce computer turnaround time of the burdensome computations.

Capillary pressure - saturation curves were determined for a Flintshot 2.8 Ottawa (medium) sand. The fluids involved were TCE and air, and TCE and water. Saturation values were determined at desired points along a 1 m long column with a dual-energy gamma radiation system. Capillary pressure values were determined at the same points from known fluid pressures at hydraulic equilibrium. Matching the saturation and capillary pressure values at a given point then resulted in P_c-S_w data points. To determine the extent of hysteresis in the P_c-S_w relationships, the wetting fluids were subjected to drainage and imbibition cycles. For both fluid systems the saturation changed rapidly with capillary pressure changes ranging from 2.5 to 10 cm. This small range of P_c -values makes the use of the standard procedure to determine P_c-S_w relationships, using a pressure/tension apparatus and a porous medium sample of often at least 5 cm in height, undesirable. Hysteresis was shown to be substantial for both fluid systems and should be accounted for in computer modeling. The pressures at which the nonwetting fluid starts to displace the wetting fluid was 6.8 cm of water for the TCE/air system and 12.8 cm for the TCE/water system. These values are not only important from a practical point of view, but also for simulation purposes. The existence of well-defined displacement pressures suggests that the use of the Brooks and Corey representation of P_c-S_w curves may be favored over the van Genuchten representation as used in this study.

A new technique was developed to accurately measure and observe the dissolution of a residual TCE phase in a uniform sand. Aqueous phase concentration measurements from the column effluent and gamma attenuation measurements suggest that the dissolving TCE phase was not mobilized as individual ganglia decreased in size. Mass transfer was shown to decrease with decreasing residual saturation, but increase with increasing water velocity, at least to a limit of $Re \approx 0.01$. A power-law model fit the data well; and although it is only valid for this particular sand, it can be used by modelers and others to (1) investigate the importance of modeling nonequilibrium dissolution and (2) aid in the estimation of the cleanup-time associated with removing TCE via dissolution.

References Cited

- Aziz, K. and A. Settari, 1979, *Petroleum Reservoir Simulation*, Applied Science Publishers, London.
- Bouloutas, E.T. and M.A. Celia, 1991, "Fast Iterative Solvers for Linear Systems Arising in the Numerical Solution of Unsaturated Flow Problems," to appear, *Advances in Water Resources*.
- Celia, M.A., L.R. Ahuja, and G.F. Pinder, 1987, "Orthogonal Collocation and Alternating-Direction Methods for Unsaturated Flow," *Advances in Water Resources*, 10, 178-187.
- Celia, M.A. and G.F. Pinder, 1990, "Generalized Alternating-Direction Collocation Methods for Parabolic Equations: 2. Transport Equations with Application to Seawater Intrusion Problems," *Numerical Methods for PDE's*, 6(3), 215-230.
- Celia, M.A., E.T. Bouloutas, and R.L. Zarba, 1990a, "A General Mass-Conservative Numerical Solution for the Unsaturated Flow Equation," *Water Resources Research*, 26, 1483-1496.
- Celia, M.A., T.F. Russell, I. Herrera, and R.E. Ewing, 1990b, "An Eulerian-Lagrangian Localized Adjoint Method for the Advection-Diffusion Transport Equation," *Advances in Water Resources*, 13, 187-206.
- Celia, M.A. and P. Binning, 1992, "Two-Phase Unsaturated Flow: One Dimensional Simulation and Air Velocities," *Water Resources Research*, in revision.
- Celia, M.A. and S. Zisman, 1990, "An Eulerian-Lagrangian Localized Adjoint Method for Reactive Transport in Groundwaters," *Invited Paper, Proc. Eight Int. Conf. Comp. Meth. Water Resources*, Gambolati et al. (eds.), Springer, 383-392.
- Cussler, E.L., 1984, *Diffusion: Mass Transfer in Fluid Systems*, Cambridge University Press, Cambridge, pages 227-228.
- Demond, A.H., and P.V. Roberts, 1991, "Effects of Interfacial Forces on Two-Phase Capillary Pressure-Saturation Relationships," *Water Resources Research*, 27(3), 423-437.
- Eppstein, M.J., J.F. Guarnaccia and D.E. Dougherty, 1992, "Parallel Groundwater Computations Using PVM," *Proceedings of the Ninth International Conference on Computational Methods in Water Resources*, Denver, June (in press).
- Ferrand, L.A., P.C.D. Milly, and G.F. Pinder, 1986, "Dual-Gamma Attenuation for the Determination of Porous Medium Saturation with Respect to Three Fluids," *Water Resources Research*, 22 (12), 1657-1663.
- Guarnaccia, J.F., 1992, Ph.D. Dissertation, Princeton University, Princeton, NJ, in preparation.
- Guarnaccia, J.F. and G.F. Pinder, 1992, "A New Two-Phase Flow and Transport Model with Interphase Mass Exchange," *Proceedings of the Ninth International Conference on Computational Methods in Water Resources*, Denver, June (in press).
- Huyakorn, P.S., and G.F. Pinder, 1983, *Computational Methods in Subsurface Flow*, Academic Press, New York, pages 156-158.
- Imhoff, P.T., Jaffé, P.R., and Pinder, G.F., 1992, "An Experimental Study of the Dissolution of Trichloroethylene in Saturated Porous Media," *Princeton University Water Resources Program Report WR-92-1*.
- Kool, J.B. and J.C. Parker, 1987, "Development and Evaluation of Closed-Form Expressions for Hysteretic Soil Hydraulic Properties," *Water Resources Research*, 23 (1), 105-114.
- Lapidus, L. and G. F. Pinder, 1982, *Numerical Solution of Partial Differential Equations in Science and Engineering*, John Wiley, New York.

Lenhard, R.J. and J.C. Parker, 1987, "Measurement and Prediction of Saturation-Pressure Relationships in Three-Phase Porous Media Systems", *Journal of Contaminant Hydrology*, 1, 407-423.

Luckner, L., M.T. van Genuchten and D.R. Nielsen, 1989, "A Consistent Set of Parametric Models for the Two-Phase Flow of Immiscible Fluids in the Subsurface," *Water Resources Research*, 25 (10), 2187-2193.

McWhorter and Sunada, 1990, "Exact Integral Solutions for Two Phase Flow," *Water Resources Research*, 26(3), 399-413.

Miller, C.T., M.M. Poirier-McNeill, and A.S. Mayer, 1990, "Dissolution of Trapped Nonaqueous Phase Liquids: Mass Transfer Characteristics," *Water Resources Research*, 26 (11), 2783-2796.

Oostrom, M., and J.H. Dane, 1990, "Calibration and Automation of a Dual-Energy Gamma System for Applications in Soil Science," *Agronomy and Soils Departmental Series No. 145*, Alabama Agricultural Experiment Station, Auburn University.

Pinder, G.F. and L.M. Abriola, 1986, "On the Simulation of Nonaqueous Phase Organic Compounds in the Subsurface," *Water Resources Research*, 22(9), 1095-1195.

Reeves, H.W. and L.M. Abriola, 1988, "A Decoupled Approach to Simulation of Flow and Transport of Non-Aqueous Organic Phase Contaminants Through Porous Media," in Celia, M. A. et al. (eds), *Computational Methods in Water Resources, Vol 1 Modelling Surface and Subsurface Flows*, New York, Elsevier, 147-152.

Turrin, R.P., 1988, "Pressure-Saturation Relations for Water, TCE and Air in Sand," *M.S. Thesis*, Princeton University.

Wilson, J.L., S.H. Conrad, W.R. Mason, W. Peplinski, and E. Hagan, 1990, "Laboratory Investigation of Residual Liquid Organics from Spills, Leaks, and Disposal of Hazardous Wastes in Groundwater," *United States Environmental Protection Agency Report EPA/600/6-90/004*, Washington, D. C.

Disclaimer

The information in this document has been funded wholly or in part by the United States Environmental Protection Agency under Cooperative Agreement CR-814946 with Princeton University. This Document has been subjected to the Agency's peer and administrative review and has been approved for publication as an EPA document.

Quality Assurance Statement

All research projects making conclusions or recommendations based on environmentally related measurements are required to participate in the Agency Quality Assurance (QA) program. This project was conducted under an approved QA project plan. The procedures specified in this plan were used without exception. Information on the plan and documentation of the QA activities are available from the respective principal investigators (J.H. Dane for the capillary pressure-saturation experiments, and P.R. Jaffe for the solubilization experiments).

United States
Environmental Protection
Agency

Center for Environmental Research
Information
Cincinnati, OH 45268

BULK RATE
POSTAGE & FEES PAID
EPA
PERMIT No. G-35

Official Business
Penalty for Private Use, \$300

Please make all necessary changes on the above label,
detach or copy, and return to the address in the upper
left-hand corner.

If you do not wish to receive these reports CHECK HERE ☐ :
detach, or copy this cover, and return to the address in the
upper left-hand corner.

EPA/600/S-92/002